

MICROCOPY

CHART

NSWC/TR-85-67

AD-A166 590

HIGHER ORDER IONOSPHERIC CORRECTIONS FOR A SPHERICALLY SYMMETRIC REFRACTING MEDIUM

BY SUSAN D. LEVINE L. RALPH GIBSON
STRATEGIC SYSTEMS DEPARTMENT

MARCH 1985

Approved for public release; distribution unlimited.



NAVAL SURFACE WEAPONS CENTER

Dahlgren, Virginia 22448-5000 • Silver Spring, Maryland 20903-5000

UNCLASSIFIED

SECURITY CLASSIFICATION OF THIS PAGE (When Data Entered)

REPORT DOCUMENTATION PAGE		READ INSTRUCTIONS BEFORE COMPLETING FORM
1 REPORT NUMBER NSWC TR 85-67	2 GOVT ACCESSION NO AD-A166590	3 RECIPIENT'S CATALOG NUMBER
4 TITLE (and Subtitle) HIGHER ORDER IONOSPHERIC CORRECTIONS FOR A SPHERICALLY SYMMETRIC REFRACTING MEDIUM		5 TYPE OF REPORT & PERIOD COVERED Final
7 AUTHOR(s) Susan D. LeVine L. Ralph Gibson		6 PERFORMING ORG REPORT NUMBER
9 PERFORMING ORGANIZATION NAME AND ADDRESS Naval Surface Weapons Center (K13) Dahlgren, VA 22448-5000		8 CONTRACT OR GRANT NUMBER(s)
11 CONTROLLING OFFICE NAME AND ADDRESS Defense Mapping Agency Washington, DC 20305		10 PROGRAM ELEMENT PROJECT TASK AREA & WORK UNIT NUMBERS MIPR
14 MONITORING AGENCY NAME & ADDRESS (if different from Controlling Office)		12 REPORT DATE March 1985
		13 NUMBER OF PAGES 30
		15 SECURITY CLASS (of this report) UNCLASSIFIED
		15a DECLASSIFICATION DOWNGRADING SCHEDULE
16 DISTRIBUTION STATEMENT (of this Report) Approved for public release; distribution unlimited		
17 DISTRIBUTION STATEMENT (of the abstract entered in Block 20, if different from Report)		
18 SUPPLEMENTARY NOTES		
19 KEY WORDS (Continue on reverse side if necessary and identify by block number) satellite tracking electromagnetic wave refraction effects refracting medium		
20 ABSTRACT (Continue on reverse side if necessary and identify by block number) Closed-form calculations for the second- and third-order ionospheric effects are presented. Single- and dual-frequency data from a NAVSAT orbit is used in the model to determine the magnitude of the corrections to the phase path and range difference for a variety of station positions. (see back)		

APR 14 1986

UNCLASSIFIED

SECURITY CLASSIFICATION OF THIS PAGE (When Data Entered)

(20)

The sum of the second- and third-order corrections to the observed range difference varied from 0.05 cm to 1.6 m for single-frequency data and from 0.09 cm to 30 cm for dual-frequency data, depending on station location and satellite zenith angle.

S N 0102-LF-014-6601

UNCLASSIFIED

SECURITY CLASSIFICATION OF THIS PAGE (When Data Entered)

FOREWORD

This report presents the results of a study to determine the magnitude of the second- and third-order ionospheric corrections to an electromagnetic wave propagating through a spherically symmetric refracting medium. The results show that both the second- and third-order correction terms must be included in a study of higher order ionospheric effects, contrary to previous reports that the second-order term is negligible. This report was reviewed by Dr. Jeffrey N. Blanton, Head, Space Flight Sciences Branch.

Released by:



THOMAS A. CLARE, Head
Strategic Systems Department

RECEIVED
3

✓
A-1

CONTENTS

	Page
INTRODUCTION	1
SECOND-ORDER CORRECTION.....	2
THIRD-ORDER CORRECTION	7
SINGLE-FREQUENCY DOPPLER DATA	7
DUAL-FREQUENCY DOPPLER DATA.....	9
NUMERICAL ANALYSIS.....	10
CORRECTIONS TO THE PHASE PATH	12
CORRECTIONS TO THE RANGE DIFFERENCE.....	16
CONCLUSIONS	19
APPENDIX--DUAL-FREQUENCY RANGE DIFFERENCE	A-1
DISTRIBUTION	(1)

INTRODUCTION

The phase path, L_ρ , is the curved path that an electromagnetic wave follows when traveling from a satellite to a receiving station. The path is curved due to refraction effects of the Earth's ionosphere.

An expansion for the phase path length takes the form

$$L_\rho = \rho + L_1 + L_2 + L_3 + \dots$$

where ρ is the vacuum slant range from the station to satellite and L_1, L_2, L_3, \dots first-, second-, third-, etc. order corrections to the phase path. By assuming the refracting medium to be spherically symmetric, a closed-form integral can be derived for L_ρ and subsequently for L_1, L_2, L_3, \dots etc. The closed-form integral expressions have been derived by Gibson¹ for the first-, second-, and third-order corrections and are dependent on the vacuum zenith angle and the index of refraction model used.

The first-order correction is given by¹

$$L_1 = 1/2 \int \frac{(n^2(r) - 1)rdr}{\sqrt{r^2 - k^2}} \quad (1)$$

where the constant k is

$$k = r_0 \sin z$$

with r_0 the distance from the center of the Earth to the station and z the vacuum zenith angle. $N(r)$ is the index of refraction of the ionosphere or plasma:

¹L. R. Gibson, *Some Expansions for an Electromagnetic Wave Propagating Through a Spherically Symmetric Refracting Medium*, Naval Surface Weapons Center Technical Report NSWC/DI TR-3344 Dahlgren, VA June, 1975.

$$n^2(r) - 1 = - \frac{\omega_p^2(r)}{\omega^2} \quad (2)$$

where $\omega_p(r)$ is the plasma frequency and²

$$\omega_p^2(r) = \frac{4\pi e^2}{m} N(r) \quad (3)$$

$N(r)$ is the electron density in electrons/cm³, e the electronic charge in statcoulombs, m the mass of the electron in grams, and ω the signal frequency in radians/s.

Substitution of Equation 2 into Equation 1 shows that the first-order correction goes as $1/\omega^2$:

$$L_1 = - 1/2 \int \frac{\omega_p^2(r) \, r \, dr}{\omega^2 \sqrt{r^2 - k^2}} \quad (4)$$

SECOND-ORDER CORRECTION

The second-order correction to the phase path length accounts for the effect of the Earth's magnetic field on the ionosphere.

The index of refraction of a plasma in an external magnetic field is:²

$$n^2(r) - 1 = \frac{-\omega_p^2(r)}{\omega(\omega \mp \omega_B(r))} \quad (5)$$

where $\omega_B(r)$ is the frequency of precession of a charged particle in a magnetic field:

$$\omega_B(r) = \frac{eB(r)}{mc} \quad (6)$$

²J. D. Jackson, *Classical Electrodynamics*, John Wiley and Sons, Inc., New York, NY, 1975

In Equation 6, e and m are as defined previously, c is the speed of light in cm/s, and $B(r)$ is the component of the Earth's magnetic field in the direction of signal propagation. From Equation 5 it can be seen that electromagnetic waves of different polarizations propagate differently.

To obtain the expression for the second-order correction, expand Equation 5:

$$n^2(r) = 1 - \left(\frac{\omega_p^2(r)}{\omega^2} \right) \left[1 \pm \frac{\omega_B(r)}{\omega} \right]^{-1}$$

$$\left[1 \pm \frac{\omega_B(r)}{\omega} \right]^{-1} = 1 \mp \frac{\omega_B(r)}{\omega} + \frac{\omega_B^2(r)}{\omega^2} \mp \frac{\omega_B^3(r)}{\omega^3} + \dots$$

$$n^2(r) - 1 = \frac{-\omega_p^2(r)}{\omega^2} \pm \frac{\omega_p^2(r) \omega_B(r)}{\omega^3} - \frac{\omega_p^2(r) \omega_B^2(r)}{\omega^4}$$

The last expression substituted into Equation 1 modifies the first-order correction:

$$\bar{L}_1 = 1/2 \left[\int \frac{-\omega_p^2(r) \, r \, dr}{\omega^2 \sqrt{r^2 - k^2}} \pm \int \frac{\omega_p^2(r) \omega_B(r) \, r \, dr}{\omega^3 \sqrt{r^2 - k^2}} \right. \\ \left. - \int \frac{\omega_p^2(r) \omega_B^2(r)}{\omega^4} \frac{r \, dr}{\sqrt{r^2 - k^2}} \right] \quad (7)$$

The first term in the expansion is just the first-order correction, L_1 , as given previously in Equation 4; the second term, which goes as $1/\omega^3$, is called the second-order correction, L_2 ; and the third term, which goes as $1/\omega^4$, is a part of the third-order correction and will be discussed later. Note that the second-order correction is the first-order correction multiplied by the precession frequency and divided by the oscillator frequency:

$$L_2 = \frac{\omega_B}{\omega} \cdot L_1 \quad (8)$$

To determine the magnitude of L_2 , it is necessary to find ω_B .

To find the precession frequency, an expression for $B(r)$ is needed in the direction of signal propagation, $\hat{\rho}$ (Figure 1).

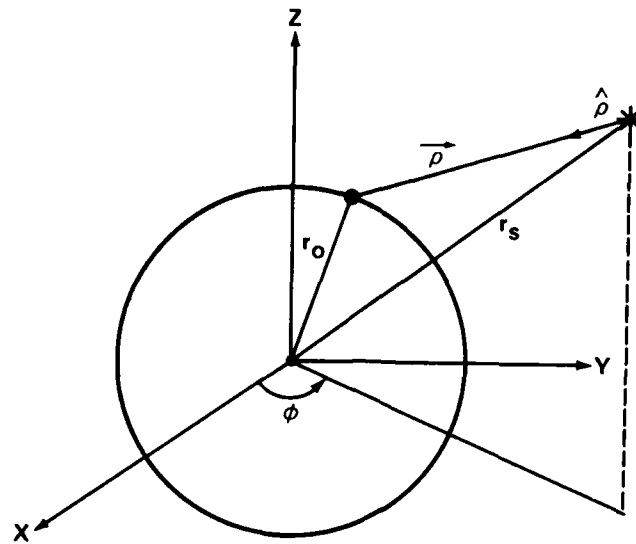


FIGURE 1. DIRECTION OF SIGNAL PROPAGATION

Given the Earth-fixed coordinates of the satellite (x_s, y_s, z_s) and station (x_o, y_o, z_o) , $\vec{\rho}$ can be defined by

$$\vec{\rho} = (x_s - x_o) \hat{x} + (y_s - y_o) \hat{y} + (z_s - z_o) \hat{z}$$

The magnetic field of the earth can be represented in geodetic coordinates as

$$\vec{B} = B_r \hat{r} + B_\theta \hat{\theta} + B_\phi \hat{\phi}$$

where B_r , B_θ , B_ϕ are also known as B_{down} , B_{north} , and B_{east} , respectively.

Therefore

$$B_\rho = \vec{B} \cdot \hat{\rho}$$

is the component of \vec{B} in the direction of signal propagation. The resulting expression for B_ρ is

$$B_\rho = \frac{1}{|\vec{\rho}|} \left[B_r [(x_s - x_o) \cos \theta \cos \phi + (y_s - y_o) \cos \theta \sin \phi + (z_s - z_o) \sin \theta] \right. \\ \left. + B_\theta [-(x_s - x_o) \sin \theta \cos \phi - (y_s - y_o) \sin \theta \sin \phi + (z_s - z_o) \cos \theta] \right. \\ \left. + B_\phi [-(x_s - x_o) \sin \phi + (y_s - y_o) \cos \phi] \right]$$

Also required before evaluation of Equation 8 can begin is a model for the electron density profile, $N(r)$, in Equation 3.

The ionosphere is composed of several distinct regions in which the functional form of $N(r)$ varies from one region to the next. Therefore, it is necessary to separate the integral in Equation 8 into a series of integrals over the different ionospheric regions:

$$L_2 = \frac{2\pi e^2 \omega_b}{m\omega^3} \left[\int_{\text{E Layer}} \frac{N_E(r) \, r \, dr}{\sqrt{r^2 - k^2}} + \int_{\text{F1 Layer}} \frac{N_{F_1}(r) \, r \, dr}{\sqrt{r^2 - k^2}} + \int_{\text{Lower F2 Layer}} \frac{N_{F_{21}}(r) \, r \, dr}{\sqrt{r^2 - k^2}} \right. \\ \left. + \int_{\text{mid-upper F2 Layer}} \frac{N_{F_{22}}(r) \, r \, dr}{\sqrt{r^2 - k^2}} + \int_{\text{1st upper F}_2 \text{ exponentially decaying layer}} \frac{N_{F_{23}}(r) \, r \, dr}{\sqrt{r^2 - k^2}} + \int_{\text{2nd upper F}_2 \text{ exponentially decaying layer}} \frac{N_{F_{24}}(r) \, r \, dr}{\sqrt{r^2 - k^2}} + \int_{\text{3rd upper F}_2 \text{ exponentially decaying layer}} \frac{N_{F_{25}}(r) \, r \, dr}{\sqrt{r^2 - k^2}} \right]$$

For the numerical analysis performed later in this report, the functional forms for the corresponding $N(r)$'s were taken from the Applied Research Laboratories (ARL) ionospheric model (Figure 2).³

³J. R. Clench and R. A. Menburg, *Ionospheric Residual Range Error Model*, Applied Research Laboratories Technical Report ARL-TR 79-9, Austin, TX, March 1979.

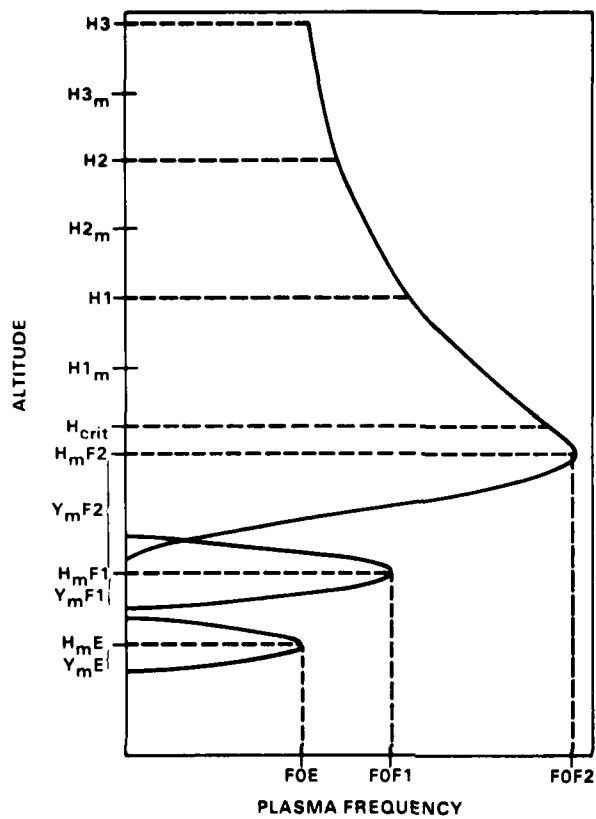


FIGURE 2. VERTICAL ELECTRON-DENSITY PROFILE

THIRD-ORDER CORRECTION

The closed-form integral expression for the third-order correction, neglecting magnetic field effects is:¹

$$\bar{L}_3 = -1/8 \left\{ \int \frac{(n^2(r) - 1)^2 r^3 dr}{(r^2 - k^2)^{3/2}} - k^2 \left[\int \frac{(n^2(r) - 1) r dr}{(r^2 - k^2)^{3/2}} \right]^2 / \int \frac{r dr}{(r^2 - k^2)^{3/2}} \right\}$$

To include the magnetic field interaction, the third term in Equation 7 must be added to the above. Substituting for $n^2(r) - 1$ and adding the magnetic field interaction term leads to the following expression for the third-order correction:

$$L_3 = -1/8 \left\{ \int \frac{\omega_p^4(r) r^3 dr}{\omega^4 (r^2 - k^2)^{3/2}} - \frac{k^2}{\omega^4} \left[\int \frac{\omega_p^2(r) r dr}{(r^2 - k^2)^{3/2}} \right]^2 / \int \frac{r dr}{(r^2 - k^2)^{3/2}} \right\} \\ - 1/2 \int \frac{\omega_p^2(r) \omega_B^2(r) r dr}{\omega^4 \sqrt{r^2 - k^2}} \quad (9)$$

The third-order correction goes as $1/\omega^4$. As before, each integral in Equation 9 must be separated into a series of integrals over the different layers of the ionosphere.

SINGLE-FREQUENCY DOPPLER DATA

For satellites emitting a single frequency, f_T , the first-, second-, and third-order ionospheric corrections can be determined directly from Equations 4, 8, and 9. Factoring out the transmitter frequency gives the following convenient form for the phase path:

$$L_\rho = \rho + \frac{1}{f_T^2} L_1 + \frac{1}{f_T^3} L_2 + \frac{1}{f_T^4} L_3$$

For Doppler data, the time derivative of the phase path is needed to calculate the received frequency, f_r .

$$f_r = (1 - \dot{L}_\rho/c) f_T \quad (10)$$

where

$$\dot{L}_\rho = \dot{\rho} + \frac{1}{f_T^2} \dot{L}_1 + \frac{1}{f_T^3} \dot{L}_2 + \frac{1}{f_T^4} \dot{L}_3$$

Expanding Equation 10 gives

$$f_r = f_T - \frac{f_T \dot{\rho}}{c} - \frac{1}{cf_T} \dot{L}_1 - \frac{1}{cf_T^2} \dot{L}_2 - \frac{1}{cf_T^3} \dot{L}_3$$

The signal received by a station, f_r , combines with a station transmitter of frequency, f_s , to get beat frequency:

$$\frac{dN}{dt} = f_s - f_r$$

where N is the number of beats.

$$f_s - f_r = f_s - f_T + \frac{f_T \dot{\rho}}{c} + \frac{1}{cf_T} \dot{L}_1 + \frac{1}{cf_T^2} \dot{L}_2 + \frac{1}{cf_T^3} \dot{L}_3$$

Define $\Delta f = f_s - f_T$

$$\frac{dN}{dt} = \Delta f + \frac{f_T}{c} \frac{d\rho}{dt} + \frac{1}{cf_T} \frac{dL_1}{dt} + \frac{1}{cf_T^2} \frac{dL_2}{dt} + \frac{1}{cf_T^3} \frac{dL_3}{dt}$$

$$N = \Delta f \Delta t + \frac{f_T \Delta \rho}{c} + \frac{1}{cf_T} \Delta L_1 + \frac{1}{cf_T^2} \Delta L_2 + \frac{1}{cf_T^3} \Delta L_3$$

Solving for the range difference, $\Delta \rho$, gives

$$\Delta \rho = \underbrace{\frac{c}{f_T} (N - \Delta f \Delta t)}_{\Delta \rho_{obs}} - \underbrace{\left(\frac{1}{f_T^2} \right) \Delta L_1}_{\Delta \rho_1} - \underbrace{\left(\frac{1}{f_T^3} \right) \Delta L_2}_{\Delta \rho_2} - \underbrace{\left(\frac{1}{f_T^4} \right) \Delta L_3}_{\Delta \rho_3} \quad (11)$$

The first term in Equation 11, $\Delta\rho_{obs}$, represents the observed uncorrected value for the range difference. The correction terms are given by $\Delta\rho_1$, $\Delta\rho_2$, and $\Delta\rho_3$.

DUAL-FREQUENCY DOPPLER DATA

Most satellites emit two signals at different frequencies, f_{T_1} and f_{T_2} , to eliminate the first-order correction.

$$\left\{ \begin{aligned} f_{r_1} &= f_{T_1} - \frac{f_{T_1}\dot{\rho}}{c} - \frac{1}{cf_{T_1}} \dot{L}_1 - \frac{1}{cf_{T_1}^2} \dot{L}_2 - \frac{1}{cf_{T_1}^3} \dot{L}_3 \end{aligned} \right. \quad (12)$$

$$\left\{ \begin{aligned} f_{r_2} &= f_{T_2} - f_{T_2} \frac{\dot{\rho}}{c} - \frac{1}{cf_{T_2}} \dot{L}_1 - \frac{1}{cf_{T_2}^2} \dot{L}_2 - \frac{1}{cf_{T_2}^3} \dot{L}_3 \end{aligned} \right. \quad (13)$$

Assume $f_{T_1} < f_{T_2}$ and define $\lambda = f_{T_1}/f_{T_2}$.

Subtracting λ times Equation 12 from Equation 13 gives

$$\begin{aligned} f_{r_2} - \lambda f_{r_1} &= (f_{T_2} - \lambda f_{T_1}) - (f_{T_2} - \lambda f_{T_1}) \frac{\dot{\rho}}{c} - \left(\frac{1}{f_{T_2}} - \frac{\lambda}{f_{T_1}} \right) \frac{\dot{L}_1}{c} \\ &\quad - \left(\frac{1}{f_{T_2}^2} - \frac{\lambda}{f_{T_1}^2} \right) \frac{\dot{L}_2}{c} - \left(\frac{1}{f_{T_2}^3} - \frac{\lambda}{f_{T_1}^3} \right) \frac{\dot{L}_3}{c} \end{aligned}$$

Substituting for λ gives

$$\begin{aligned} f_{r_2} - \frac{f_{T_1} f_{r_1}}{f_{T_2}} &= (f_{T_2} - f_{T_1}^2/f_{T_2}) - (f_{T_2} - \frac{f_{T_1}^2}{f_{T_2}}) \frac{\dot{\rho}}{c} \\ &\quad - \left(\frac{1}{f_{T_2}^2} - \frac{1}{f_{T_1} f_{T_2}} \right) \frac{\dot{L}_2}{c} - \left(\frac{1}{f_{T_2}^3} - \frac{1}{f_{T_1}^2 f_{T_2}} \right) \frac{\dot{L}_3}{c} \end{aligned}$$

Define $f_{T_c} = f_{T_2} - f_{T_1}^2/f_{T_2}$

Then the frequency received by the station is

$$f_{r_e} = f_{r_2} - \lambda f_{r_1} = f_{T_e} (1 - \dot{\rho}/c) - \left(\frac{1}{f_{T_2}^2} - \frac{1}{f_{T_1} f_{T_2}} \right) \frac{\dot{L}_2}{c} - \left(\frac{1}{f_{T_2}^3} - \frac{1}{f_{T_1}^2 f_{T_2}} \right) \frac{\dot{L}_3}{c}$$

To determine the range difference for dual-frequency data, the same analysis as for the single-frequency case is followed. The result (see the appendix) is given below:

$$\Delta\rho = \underbrace{\frac{c}{f_{T_e}} (N - \Delta f \Delta t)}_{\Delta\rho_{obs}} + \underbrace{\frac{1}{(f_{T_1} + f_{T_2}) (f_{T_1} f_{T_2})}}_{\Delta\rho_2} \Delta L_2 + \underbrace{\frac{1}{f_{T_1}^2 f_{T_2}^2}}_{\Delta\rho_3} \Delta L_3$$

NUMERICAL ANALYSIS

A numerical analysis was performed to determine the magnitude of the second- and third-order corrections to the phase path and also to the range difference.

A FORTRAN program was written to perform the calculations and interfaced with another program that contained the ARL model. The combined program uses the Earth-fixed coordinates of the satellite and the given station position to determine the slant range, ρ , at given time intervals for a pass over the station. The various ionospheric parameters needed by the ARL model, along with the magnetic field components, are evaluated at the point on ρ that is 350 km above the Earth. This particular height was chosen after numerical integrations showed it to give the best average fit for the parameters along ρ . A simplified flowchart of the combined program is given in Figure 3.

A NAVSAT orbit provided the data for the analysis. Results were obtained for three stations:

1. Near the North Pole
2. Mid-latitude
3. Near the equator

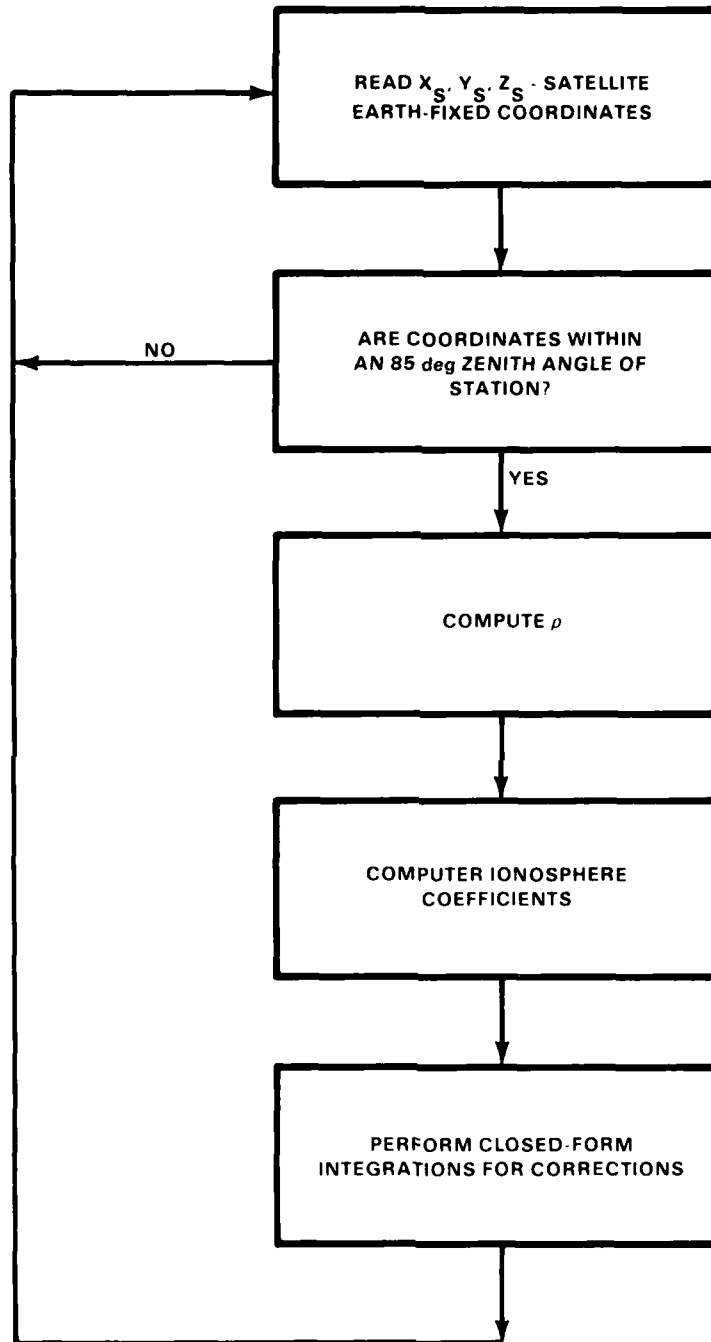


FIGURE 3. COMBINED PROGRAM FLOWCHART

<u>Station Number</u>	<u>Location</u>
118	Thule, Greenland
30280	Santiago, Chile
30121	Quito, Ecuador

For the analysis, a relatively high sunspot number of 137 was assumed. For the single-frequency case, the frequency was taken to be 150 MHz; for the dual-frequency case, the assigned frequencies were 150 and 400 MHz.

CORRECTIONS TO THE PHASE PATH

For single-frequency data, the sum of the second- and third-order corrections to the phase path varied from -24 cm to -10 m, depending on station location and satellite zenith angle. For two frequencies the sum of the corrections is less, varying from -2.5 cm to -1.3 m.

The second-order correction was found to be much larger than the third-order correction for many points along the pass. This was especially evident for station 118 (Thule, Greenland) where, for small satellite zenith angles, the second-order correction was nearly 27 times larger than the third-order correction for the single-frequency case and almost 20 times larger for the dual-frequency case. This is not unexpected since the magnetic field contribution to the precession frequency along ρ is larger here.

For the single-frequency case at station 30280 (mid-latitude), the second-order correction was approximately 5 times larger than the third-order correction for many points along the pass, decreasing to 1.5 times as large at other points, and becoming 3.7 times less at one point. The dual-frequency case showed the second- and third-order corrections to be about equal in magnitude at many points along the pass, with the second-order correction becoming approximately 3.5 times larger than the third-order correction at other points, and 5 times less at one point along the pass.

The results for station 30121 (equator) showed the second-order correction to be from 3.5 to 10.5 times larger than the third-order correction for most points along the pass and approximately 3 times less at one point for the single-frequency case. For two frequencies, the second-order varied from 2.5 to 7.6 times larger and approximately 4 times less at one point.

Tables 1 through 3 give a complete listing of the results for the phase path corrections.

TABLE 1. PHASE PATH CORRECTIONS,
STATION 118

Zenith Angle	Single Frequency			Dual Frequency	
	L ₁ (m)	L ₂ (m)	L ₃ (m)	L ₂ (m)	L ₃ (m)
83.81	-556.5431	-1.5854	-0.2581	-0.1621	-0.0363
79.36	-537.8851	-1.7190	-0.2290	-0.1758	-0.0322
74.03	-552.5074	-2.0435	-0.2312	-0.2090	-0.0325
67.34	-514.4646	-2.2670	-0.1976	-0.2318	-0.0278
58.50	-444.0260	-2.3880	-0.1548	-0.2442	-0.0218
46.26	-369.1418	-2.4530	-0.1208	-0.2509	-0.0170
29.34	-308.2193	-2.4730	-0.0999	-0.2530	-0.0140
13.07	-279.5940	-2.4470	-0.0908	-0.2503	-0.0128
25.42	-292.3383	-2.3550	-0.0915	-0.2409	-0.0129
43.47	-337.6948	-2.2080	-0.1022	-0.2259	-0.0144
56.78	-399.6440	-2.0367	-0.1242	-0.2083	-0.0175
66.32	-470.9486	-1.8750	-0.1609	-0.1918	-0.0226
73.45	-538.8791	-1.7042	-0.2111	-0.1743	-0.0297
79.07	-594.6678	-1.5250	0.2710	-0.1559	-0.0381
83.72	-634.7061	-1.3470	-0.3304	-0.1378	-0.0465

TABLE 2. PHASE PATH CORRECTIONS,
STATION 30280

<u>Zenith Angle</u>	<u>Single Frequency</u>			<u>Dual Frequency</u>	
	<u>L₁ (m)</u>	<u>L₂ (m)</u>	<u>L₃ (m)</u>	<u>L₂ (m)</u>	<u>L₃ (m)</u>
82.65	-971.2966	-4.3526	-1.0043	-0.4452	-0.1412
78.37	-1027.0405	-4.5764	-1.0634	-0.4680	-0.1495
73.41	-1044.3015	-4.6496	-1.0451	-0.4755	-0.1470
67.49	-1016.6601	-4.5264	-0.9639	-0.4629	-0.1355
60.20	-953.4671	-4.2193	-0.8585	-0.4315	-0.1207
50.94	-874.2020	-3.7739	-0.7564	-0.3860	-0.1064
38.97	-793.8011	-3.1973	-0.6733	-0.3270	-0.0947
23.99	-734.1684	-2.5000	-0.6260	-0.2556	-0.0880
10.47	-725.5116	-1.6963	-0.6399	-0.1735	-0.0900
19.62	-788.6913	-0.7774	-0.7458	-0.0795	-0.1048
35.38	-934.0459	-0.2675	-0.9817	-0.0274	-0.1381
48.42	-1148.6793	-1.4604	-1.3891	-0.1494	-0.1953
58.52	-1413.5384	-2.7990	-2.0193	-0.2862	-0.2840
66.41	-1698.1758	-4.2300	-2.8959	-0.4326	-0.4072
72.75	-1946.6436	-5.5975	-3.8845	-0.5725	-0.5463
78.01	-2068.1360	-6.5857	-4.5026	-0.6735	-0.6332
82.52	-1967.8629	-6.7961	-4.1003	-0.6951	-0.5766

TABLE 3. PHASE PATH CORRECTIONS,
STATION 30121

<u>Zenith Angle</u>	<u>Single Frequency</u>			<u>Dual Frequency</u>	
	<u>L₁ (m)</u>	<u>L₂ (m)</u>	<u>L₃ (m)</u>	<u>L₂ (m)</u>	<u>L₃ (m)</u>
83.97	-1040.172	-6.0897	-1.1466	-0.6228	-0.1612
79.31	-911.7480	-5.2910	-0.8206	-0.5411	-0.1154
73.71	-779.4886	-4.4729	-0.5646	-0.4575	-0.0794
66.70	-654.9483	-3.6845	-0.3920	-0.3768	-0.0551
57.54	-544.7377	-2.9351	-0.2804	-0.3002	-0.0394
45.23	-451.9222	-2.1968	-0.2089	-0.2247	-0.0294
29.65	-386.7652	-1.4543	-0.1673	-0.1987	-0.0235
18.93	-368.6050	-0.7083	-0.1562	-0.0724	-0.0220
29.14	-403.8287	-0.0628	-0.1791	-0.6425 x 10 ⁻²	-0.0252
44.21	-485.389	-0.8599	-0.2386	-0.0879	-0.0336
56.13	-596.9806	-1.6775	-0.3366	-0.1716	-0.0473
65.03	-722.1351	-2.4898	-0.4784	-0.2546	-0.0673
71.86	-859.1412	-3.3015	-0.6814	-0.3377	-0.0958
77.33	-1018.9937	-4.167	-0.9980	-0.4261	-0.1403
81.90	-1226.4705	-5.2009	-1.546	-0.5319	-0.2174

CORRECTIONS TO THE RANGE DIFFERENCE

The second- and third-order range difference corrections were determined by taking the difference in the phase path corrections at two successive points along the pass. The sum of the second- and third-order range difference corrections varied from as little as 0.05 cm to -1.6 m for the single-frequency case and from 0.09 cm to approximately 30 cm for dual-frequency data. Tables 4 through 6 give the corrections to the range difference for the three stations.

TABLE 4. RANGE DIFFERENCE RESULTS,
STATION 118

Zenith Angles for Which Difference was Computed	Single Frequency			Dual Frequency	
	$\Delta\rho_1$ (m)	$\Delta\rho_2$ (m)	$\Delta\rho_3$ (m)	$\Delta\rho_2$ (m)	$\Delta\rho_3$ (m)
83.81, 79.36	18.6580	-0.1337	0.0291	-0.0137	0.4094×10^{-2}
79.36, 74.03	-14.6222	-0.3244	0.2180×10^{-2}	-0.0332	-0.3066×10^{-3}
74.03, 67.34	38.0428	-0.2234	0.0336	-0.0228	0.4724×10^{-2}
67.34, 58.50	70.4386	-0.1212	0.0428	-0.0124	0.6020×10^{-2}
58.50, 46.26	74.8842	-0.0651	0.0339	-0.6662×10^{-2}	0.4772×10^{-2}
46.26, 29.34	60.9225	-0.0205	0.0210	-0.2101×10^{-2}	0.2956×10^{-2}
29.34, 13.07	28.6253	0.0259	0.9014×10^{-2}	0.2651×10^{-2}	0.1267×10^{-2}
13.07, 25.43	-12.7442	0.0925	-0.6906×10^{-3}	0.9464×10^{-2}	-0.9713×10^{-4}
25.43, 43.47	-45.3565	0.1470	-0.0106	0.01503	-0.1496×10^{-2}
43.47, 56.78	-61.9492	0.1717	-0.0221	0.0176	-0.3102×10^{-2}
56.78, 66.32	-71.3046	0.1615	-0.0367	0.0165	-0.5159×10^{-2}
66.32, 73.45	-67.9305	0.1710	-0.0501	0.0175	-0.7050×10^{-2}
73.45, 79.07	-55.7087	0.1796	-0.0599	0.0184	-0.8423×10^{-2}
79.07, 83.72	-40.0383	0.1772	-0.0594	0.0181	-0.8358×10^{-2}

TABLE 5. RANGE DIFFERENCE RESULTS,
STATION 30280

Zenith Angles for Which Difference was Computed	Single Frequency			Dual Frequency	
	$\Delta\rho_1$ (m)	$\Delta\rho_2$ (m)	$\Delta\rho_3$ (m)	$\Delta\rho_2$ (m)	$\Delta\rho_3$ (m)
82.65, 78.37	- 55.7439	-0.2238	-0.0591	-0.0229	-0.8314 x 10 ⁻²
78.37, 73.41	- 17.2610	-0.0732	0.0183	-0.7489 x 10 ⁻²	0.2577 x 10 ⁻²
73.41, 67.49	27.6414	0.1232	0.0812	0.0126	0.0114
67.49, 60.20	63.1930	0.3071	0.1054	0.0314	0.0148
60.20, 50.94	79.2651	0.4454	0.1021	0.0456	0.0144
50.94, 38.97	80.4009	0.5766	0.0831	0.0590	0.0117
38.97, 23.99	59.6327	0.6977	0.0473	0.0714	0.6650 x 10 ⁻²
23.99, 10.47	8.6568	0.8033	-0.0139	0.0822	-0.1958 x 10 ⁻²
10.47, 19.62	- 63.1797	0.9189	-0.1058	0.0940	-0.0149
19.62, 35.38	-145.3545	0.5098	-0.2360	0.0521	-0.0332
35.38, 48.42	-214.6334	-1.193	-0.4073	-0.1220	-0.0573
48.42, 58.52	-264.8591	-1.338	-0.6302	-0.1369	-0.0886
58.52, 66.41	-284.6374	-1.4315	-0.8766	-0.1464	-0.1233
66.41, 72.75	-248.4678	-1.3675	-0.9886	-0.1399	-0.1390
72.75, 78.01	-121.4924	-0.9882	-0.6181	-0.1011	-0.0869
78.01, 82.52	100.2731	-0.2103	0.4023	-0.0215	0.0566

TABLE 6. RANGE DIFFERENCE RESULTS,
STATION 30121

Zenith Angles for Which Difference was Computed	Single Frequency			Dual Frequency	
	$\Delta\rho_1$ (m)	$\Delta\rho_2$ (m)	$\Delta\rho_3$ (m)	$\Delta\rho_2$ (m)	$\Delta\rho_3$ (m)
83.97, 79.31	128.4244	0.7987	0.3259	0.0817	0.0458
79.31, 73.71	132.2593	0.8181	0.2560	0.0837	0.0360
73.71, 66.70	124.5403	0.7884	0.1727	0.0806	0.0243
66.70, 57.54	110.2106	0.7494	0.1116	0.0766	0.0157
57.54, 45.23	92.8155	0.7383	0.0715	0.0755	0.0101
45.23, 29.65	65.1570	0.7426	0.0416	0.0759	0.5844×10^{-2}
29.65, 18.93	18.1603	0.7460	0.0111	0.0763	0.1564×10^{-2}
18.93, 29.14	- 35.2238	0.6455	-0.0229	0.0660	-0.3222×10^{-2}
29.14, 44.21	- 81.5605	-0.7971	-0.0595	-0.0815	-0.8364×10^{-2}
44.21, 56.13	-111.5914	-0.8175	-0.0980	-0.0836	-0.0138
56.13, 65.03	-125.1545	-0.8124	-0.1417	-0.0831	-0.0199
65.03, 71.86	-137.0061	-0.8117	-0.2030	-0.0830	-0.0285
71.86, 77.33	-159.8525	-0.8651	-0.3166	-0.0885	-0.0445
77.33, 81.90	-207.4769	-1.0343	-0.5477	-0.1057	-0.0770

CONCLUSIONS

As a result of this study, the authors have concluded that when considering higher order ionospheric effects, both second and third order must be considered: neither one can be neglected.

In the near future the authors are planning to merge their coding for the ionosphere model with a new orbit determination program (OMNIS) that is currently being developed by the Space and Surface Systems Division at NSWC. With this coding included, one will have the option of computing higher order effects if desired. Also in the rare case when a satellite loses one of its signals, the model can be used to calculate a first-order ionospheric correction.

A technical report fully describing the model and range corrections will be published in the near future.

NSWC TR 85-67

APPENDIX
DUAL-FREQUENCY RANGE DIFFERENCE

$$\begin{cases} f_{r_1} = f_{T_1} - \frac{f_{T_1} \dot{\rho}}{c} - \frac{1}{cf_{T_1}} \dot{L}_1 - \frac{1}{cf_{T_1}^2} \dot{L}_2 - \frac{1}{cf_{T_1}^3} \dot{L}_3 \\ f_{r_2} = f_{T_2} - \frac{f_{T_2} \dot{\rho}}{c} - \frac{1}{cf_{T_2}} \dot{L}_1 - \frac{1}{cf_{T_2}^2} \dot{L}_2 - \frac{1}{cf_{T_2}^3} \dot{L}_3 \end{cases}$$

Define $\lambda = f_{T_1}/f_{T_2}$

$$\begin{aligned} f_{r_2} - \lambda f_{r_1} &= \left(f_{T_2} - \frac{f_{T_1}^2}{f_{T_2}} \right) - \left(f_{T_2} - \frac{f_{T_1}^2}{f_{T_2}} \right) \frac{\dot{\rho}}{c} \\ &\quad - \left(\frac{1}{f_{T_2}^2} - \frac{1}{f_{T_1} f_{T_2}} \right) \frac{\dot{L}_2}{c} - \left(\frac{1}{f_{T_2}^3} - \frac{1}{f_{T_1}^2 f_{T_2}} \right) \frac{\dot{L}_3}{c} \end{aligned}$$

Define $f_{r_e} = \left(f_{r_2} - \lambda f_{r_1} \right)$ $f_{T_e} = \left(f_{T_2} - \frac{f_{T_1}^2}{f_{T_2}} \right) = \frac{f_{T_2}^2 - f_{T_1}^2}{f_{T_2}}$

$$f_{r_e} = f_{T_e} \left(1 - \frac{\dot{\rho}}{c} \right) - \left(\frac{1}{f_{T_2}^2} - \frac{1}{f_{T_1} f_{T_2}} \right) \frac{\dot{L}_2}{c} - \left(\frac{1}{f_{T_2}^3} - \frac{1}{f_{T_1}^2 f_{T_2}} \right) \frac{\dot{L}_3}{c}$$

Define $\Delta f = f_s - f_{T_e}$

$$\frac{dN}{dt} = f_s - f_{T_e} = \Delta f + f_{T_e} \frac{\dot{\rho}}{c} + \left(\frac{1}{f_{T_2}^2} - \frac{1}{f_{T_1} f_{T_2}} \right) \frac{\dot{L}_2}{c} + \left(\frac{1}{f_{T_2}^3} - \frac{1}{f_{T_1}^2 f_{T_2}} \right) \frac{\dot{L}_3}{c}$$

$$N = \Delta f \Delta t + \frac{f_{T_e} \Delta \rho}{c} + \left(\frac{1}{f_{T_2}^2} - \frac{1}{f_{T_1} f_{T_2}} \right) \frac{\Delta L_2}{c} + \left(\frac{1}{f_{T_2}^3} - \frac{1}{f_{T_1}^2 f_{T_2}} \right) \frac{\Delta L_3}{c}$$

$$\frac{c}{f_{T_e}} (N - \Delta f \Delta t) - \frac{1}{f_{T_e}} \left(\frac{1}{f_{T_2}^2} - \frac{1}{f_{T_1} f_{T_2}} \right) \Delta L_2 - \frac{1}{f_{T_e}} \left(\frac{1}{f_{T_2}^3} - \frac{1}{f_{T_1}^2 f_{T_2}} \right) \Delta L_3 = \Delta \rho$$

ΔL_2 coefficient:

$$\frac{1}{f_{T_e}} \left(\frac{1}{f_{T_2}^2} - \frac{1}{f_{T_1} f_{T_2}} \right) = - \frac{1}{(f_{T_1} + f_{T_2})(f_{T_1} f_{T_2})}$$

ΔL_3 coefficient:

$$\frac{1}{f_{T_e}} \left(\frac{1}{f_{T_2}^3} - \frac{1}{f_{T_2}^2 f_{T_1}} \right) = - \frac{1}{f_{T_1}^2 f_{T_2}^2}$$

Therefore

$$\Delta \rho = \frac{c}{f_{T_e}} (N - \Delta f \Delta t) + \frac{1}{(f_{T_1} + f_{T_2})(f_{T_1} f_{T_2})} \cdot \Delta L_2 + \frac{1}{(f_{T_1}^2 f_{T_2}^2)} \cdot \Delta L_3$$

DISTRIBUTION

	Copies		Copies
Library of Congress ATTN: Gift and Exchange Division Washington, DC 20540	4	Office of Naval Research Physical Sciences Division 800 N. Quincy St. Arlington, VA 22217	2
National Aeronautics and Space Admin. Scientific & Technical Library Code NHS 22, Rm. BA39 600 Independence Ave., SW Washington, DC 20546	2	Air Force Geophysics Laboratory Hanscom Field Bedford, MA 01731	2
Defense Mapping Agency U.S. Naval Observatory Washington, DC 20305	3	U.S. Geological Survey ATTN: Paul Needham Reston, VA 22091	2
Defense Mapping Agency Hydrographic/Topographic Center ATTN: Robert Ziegler Washington, DC 20315	10	National Oceanic & Atmospheric Admin. National Ocean Survey ATTN: Dr. John Bossler Dr. William Strange Dr. Larry Hothem Rockville, MD 20850	1 1 1 2
Defense Mapping Agency Aerospace Center ATTN: Dr. Robert Ballew St. Louis, MO 63118	8	Goddard Space Flight Center ATTN: Dr. David Smith Mr. James Marsh Dr. Joseph Siry Greenbelt, MD 20771	1 1 1 2
NAVELEX Commander, Space and Naval Warfare Systems Command Washington, DC 20363-5100	3	Jet Propulsion Laboratory ATTN: Dr. William Melbourne Pasadena, CA 91103	1 2
Naval Research Laboratory ATTN: Mr. Al Bartholomew Washington, DC 20375	4		
Naval Oceanographic Office Bay St. Louis, MS 39522	2		

DISTRIBUTION (Continued)

	Copies		Copies
The Ohio State University Dept. of Geodetic Sciences 1958 Neil Ave. ATTN: Dr. Richard Rapp Dr. Ivan Mueller Dr. Urho Uotila Columbus, OH 43210	1 1 1	Naval Space Surveillance System Dahlgren, VA 22448 Headquarters Space Division (AFSC) Los Angeles Air Force Station Box 92960 Worldway Postal Center Los Angeles, CA 90009	2 1
The University of Texas at Austin ATTN: Dr. Byron Tapley Austin, TX 78712	1 2	Physical Sciences Laboratory New Mexico State University Box 3 - PSL ATTN: Dan Martin Las Cruces, NM 88003	 3
Applied Research Laboratory University of Texas ATTN: Dr. Arnold Tucker Dr. George Born Dr. Bob Schultz Austin, TX 78712	1 1 1 4	Department of Physics Ohio University ATTN: Dr. James Dilley Athens, OH 45701	 3
Institute for Laboratory Astrophysics University of Colorado ATTN: Dr. Peter Bender Boulder, CO 80309	1	Charles Stark Draper Lab., Inc. ATTN: Paul J. Cefola Cambridge, MA 01776	 1
U.S. Naval Observatory ATTN: W. L. Klepczynski D. D. McCarthy Washington, DC 20360	1 1	Department of Physics Eastern Illinois University ATTN: Dr. William Butler Dr. P. Scott Smith Charleston, IL 61920	 1 1 4
Massachusetts Institute of Technology ATTN: Peter Morgan Cambridge, MA 02139	1	Naval Space Command Dahlgren, VA 22448	 5
Defense Mapping School Ft. Belvoir, VA 22060	3	National Geodetic Survey Gravity, Astronomy & Satellite Branch ATTN: William E. Carter Clyde Goad Rockville, MD 20052	 1 1
U. S. Navy Astronautics Group Point Mugu, CA 93041	2		

DISTRIBUTION (Continued)

Copies

Applied Physics Laboratory
Johns Hopkins University
Johns Hopkins Road
ATTN: Harold Black
 Vincent Pisacane
Laurel, MD 20707

1

2

E-OIR Measurements, Inc.
P. O. Box 3348
College Station
ATTN: J. R. Moulton
 Pat Chappell
Fredericksburg, VA 22402

1

1

Internal Distribution

E31 (GIDEP)
E211 (Green)
E231
F14
K10
K12
K13
K14

1

1

10

4

1

10

40

5

END
FILMED

5-86

DTIC